Critical behavior of the three-dimensional Ising model with anisotropic bond randomness at the ferromagnetic-paramagnetic transition line

T. Papakonstantinou and A. Malakis

Department of Physics, Section of Solid State Physics, University of Athens, Panepistimiopolis, Zografou, Athens GR 15784, Greece

(Received 3 August 2012; revised manuscript received 22 November 2012; published 23 January 2013)

We study the $\pm J$ three-dimensional (3D) Ising model with a spatially uniaxial anisotropic bond randomness on the simple cubic lattice. The $\pm J$ random exchange is applied on the xy planes, whereas, in the z direction, only a ferromagnetic exchange is used. After sketching the phase diagram and comparing it with the corresponding isotropic case, the system is studied at the ferromagnetic-paramagnetic transition line using parallel tempering and a convenient concentration of antiferromagnetic bonds ($p_z = 0$; $p_{xy} = 0.176$). The numerical data clearly point out a second-order ferromagnetic-paramagnetic phase transition belonging in the same universality class with the 3D random Ising model. The smooth finite-size behavior of the effective exponents, describing the peaks of the logarithmic derivatives of the order parameter, provides an accurate estimate of the critical exponent $1/\nu = 1.463(3)$, and a collapse analysis of magnetization data gives an estimate of $\beta/\nu = 0.516(7)$. These results are in agreement with previous papers and, in particular, with those of the isotropic $\pm J$ three-dimensional Ising model at the ferromagnetic-paramagnetic transition line, indicating the irrelevance of the introduced anisotropy.

DOI: 10.1103/PhysRevE.87.012132 PACS number(s): 05.50.+q, 75.10.Nr, 64.60.Cn, 75.10.Hk

I. INTRODUCTION

Ising spin-glass models yield phase diagrams with distinctively complex ordered phases in $d = 3$. These models, although relatively simple in their formulation, have been proposed to describe complex systems, exhibiting frustration, e.g., materials, such as $Fe_{1-xi}Mn_{xi}TiO_3$ and $Eu_{1-x}Ba_xMnO_3$ [1–3], neural networks [4], etc.

The simplest of such models, but most influential over the years, is the Edwards-Anderson model [5,6], defined by the Hamiltonian,

$$H = -\sum_{\langle ij\rangle} J_{ij} s_i s_j, \tag{1}$$

where the summation is over nearest neighbors, $s = \pm 1$, and J_{ij} denotes the uncorrelated quenched exchange interaction. There are two popular random disorder distributions, the Gaussian distribution of random bonds with zero mean and unity standard deviation and the bimodal distribution of J_{ij}, given by

$$P(J_{ij}) = p\delta(J_{ij} + 1) + (1 - p)\delta(J_{ij} - 1). \tag{2}$$

Recently, the spatially uniaxial anisotropic $d = 3$ spin-glass system has been solved exactly on a hierarchical lattice by Güven *et al.* [7]. Their general study revealed a rich phase diagram topology and several new interesting features. This anisotropic spin-glass model is also the subject of this paper and is defined by the Hamiltonian,

$$H = -\sum_{u}\sum_{\langle ij\rangle_u} J_{ij}^u s_i s_j, \tag{3}$$

where the exchange interactions are uncorrelated quenched random variables, taking the values $\pm J^{xy}$ on the xy planes and the values $\pm J^z$ on the z axis. Accordingly, the bimodal distribution of J_{ij}^u takes the more general form

$$P\left(J_{ij}^u\right) = p_u\delta\left(J_{ij}^u + J^u\right) + (1 - p_u)\delta\left(J_{ij}^u - J^u\right), \tag{4}$$

where u denotes the z axis ($u = z$) or the xy planes ($u = xy$), J^u denotes the corresponding exchange interaction strength, and p_u are the probabilities of two neighboring spins (ij), having antiferromagnetic interaction.

The standard isotropic model, defined by Eqs. (1) and (2), corresponds to $J^z = J^{xy} = J(=1)$ and $p_z = p_{xy}$. The global phase diagram of this model separates three distinctive phases, ferromagnetic, paramagnetic, and glassy phases. All transitions among these phases are believed to be of second order and to belong to different universality classes. The phase diagram of the isotropic model will be presented in Sec. III A together with the corresponding phase diagram for the anisotropic model considered in this paper.

For the isotropic model, several accurate studies have been carried out to determine the critical behaviors along the transition lines for the finite-temperature phase transitions [8–27]. Most of these studies concern the ferromagnetic-paramagnetic (FP) and the glassy-paramagnetic (GP) lines. There also was a recent study for the ferromagnetic-glassy (FG) transition line [8]. The transition lines meet in a multicritical point located along the Nishimori line [18–27].

The FP transition line starts at the pure Ising model ($p = 0$) for which all critical properties have been extensively studied, and a recent very accurate estimate of the correlation length exponent is $\nu = 0.630\,02(10)$ [28–33]. As shown by Hasenbusch *et al.* [9], the introduction of the $\pm J$ quenched randomness changes the universality of the model along the FP line to that of the random Ising model (RIM) or the randomly diluted Ising model [9,16,34] in which several spin models appear to belong. These include models, such as the randomly sited and bond diluted, the random bond [35–39], the random bond Blume-Capel [40] model, and, of course, the already mentioned isotropic $\pm J$ three-dimensional Ising model at the ferromagnetic-paramagnetic transition line [9]. An accurate estimate of the correlation length exponent for these $d = 3$ FP transitions, characterizing the RIM universality class, is that given by Ref. [35] $\nu = 0.6837(53)$.

For the GP transition line, most of the work has been curried out at $p = \frac{1}{2}$ [11,13–15,41–53]. However, because of severe inherent difficulties due to both strong frustration and disorder effects in this region, there is a large spread in the

estimates of critical exponents, and some questions related to universality remain. This is clearly reflected in Table I of Katzgraber *et al.* [11] in which one can observe a large spread in the correlation length exponent and critical temperature estimates. From this paper, we quote the estimates $\nu = 2.39(5)$ and $T_c = 1.120(4)$, which apply to the present isotropic $\pm J$ spin-glass model. More recent estimates are $\nu = 2.45(15)$ and $T_c = 1.109(10)$ [10]. Finally, for the FG transitions, Ceccarelli *et al.* [8] have estimated the correlation length exponent to be $\nu = 0.96(2)$. Additional features [7,8,25,26,54–56] of the global phase diagram of the isotropic model will be discussed in Sec. III A.

The present paper is part of a research program to study, by Monte Carlo (MC) methods, the general spatially uniaxial anisotropic $d = 3$ spin-glass system considered by Güven *et al.* [7] and defined by Eqs. (3) and (4). The main motivation is to provide numerical evidence for the universality question by investigating possible effects caused by the introduced anisotropy on the critical exponents along the three different transition lines. Our first attempt here concerns the model $p_z = 0;\ p_{xy} \leqslant \frac{1}{2}$ with $J^z = J^{xy} = J(=1)$. For this model, we will present an approximate sketch of the global phase diagram and then will focus on the nature of the corresponding FP transition by carrying out a detailed numerical study at the particular case of $p_z = 0;\ p_{xy} = 0.176$.

The rest of the paper is laid out as follows: In the following subsection, we give a description of our numerical approach, utilized to derive numerical data for large ensembles of realizations of the disorder distribution and lattices with linear sizes in the range of $L \in \{8\text{–}44\}$. In Sec. II B, the finite-size scaling (FSS) scheme is described. Then, in Sec. III A, we present the phase diagrams of both isotropic and anisotropic models, and for the latter, we present the numerical evidence on which it is approximately constructed. In Sec. III B, we present all our FSS attempts for the case od $p_{xy} = 0.176$. This FSS study provides good estimates of all critical exponents and verifies that the present anisotropic model belongs to the universality class of the RIM. Our conclusions are summarized in Sec. IV.

II. MONTE CARLO SIMULATIONS AND FINITE-SIZE SCALING SCHEME

A. Monte Carlo method

In the present paper, we use our recent approach to disordered systems [40], based on a parallel tempering (PT) practice. Our PT protocol uses adequate numbers of the Metropolis *et al.* [57] sweeps of the lattice, and PT exchange moves between neighboring temperatures as detailed below. We mention here that parallel tempering combined with the Metropolis algorithm has also been used by Ceccarelli *et al.* [8] in their study of the FG transition. Furthermore, as pointed out by Hasenbusch *et al.* [9] in their study of the isotropic case, the Metropolis algorithm may be more effective than cluster dynamics for intermediate lattice sizes as a result of frustration effects present in the $\pm J$ models.

Our PT protocol has been described in detail in our recent papers [40,58], and only a brief summary is given here. For the estimation of the critical properties, we generate MC data that cover several finite-size anomalies of systems with linear size L. The PT approach is carried over to a certain temperature range depending on the lattice size. These temperatures are selected in such a way that the exchange rate is 0.5 using a practice similar to that suggested in Ref. [59]. The appropriate temperature sequences were generated via short preliminary runs in which we applied a simple histogram method [60–62] to determine, from the energy probability density functions, the temperatures, satisfying the above exchange condition [40,59]. The preliminary runs cover several disorder realizations, and the average over the temperature sequences provides us with a protocol with very small variation in the exchange rate condition as one moves from one realization to the other.

The MC scheme was carefully tested for all lattice sizes before its implementation for the generation of MC data. These tests included the estimation of the MC times necessary for the equilibration and the thermal averaging process applied to a particular disorder realization and the observation of running sample averages of several thermodynamic quantities, such as the magnetization or the susceptibility at a temperature close to criticality. The computational effort, necessary for the estimation of the critical behavior in the case of $p_z = 0;\ p_{xy} = 0.176$, was quite substantial. As mentioned earlier, MC data were generated for lattices with linear sizes in the range of $L \in \{8\text{–}44\}$. Selected tests together with all the simulation conditions appear below.

In Fig. 1, we illustrate the well-equilibrated thermal process of the system. For each lattice size and a temperature close to the critical temperature, one disorder realization was tested by observing the relaxation curves of the measurement process of the relevant thermodynamic quantities. Figure 1 presents such a relaxation process. This figure illustrates the behavior of cumulative moving averages ($M = \langle |M| \rangle_t$, with $t = 1, \ldots, t_m$) for the measurement process of the magnetization, corresponding to the largest lattice $L = 44$. We point out here that measurements of relevant thermodynamic quantities were

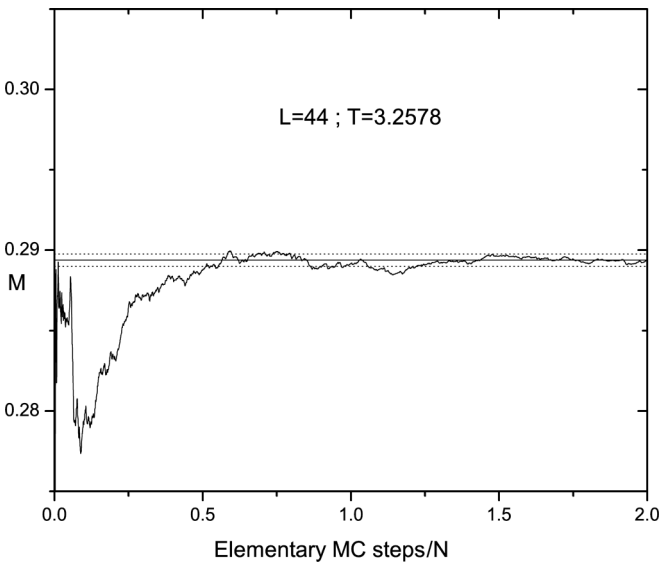

FIG. 1. Relaxation curve, illustrating the behavior of cumulative moving averages for the measurement of the magnetization during the thermal process.

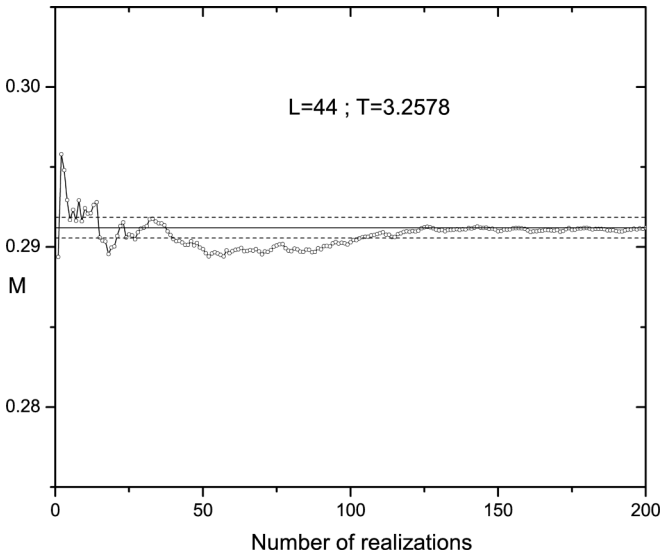

FIG. 2. Relaxation curve, illustrating the behavior of cumulative moving averages of a total of 200 realizations for the sample averaging process of the magnetization.

obtained at the end of each elementary MC step. Such an elementary MC step consisted of a PT exchange attempt followed by a full Metropolis sweep of the lattice ($N = L^3$ spin flip attempts). In a convenient notation, we use the pair $(t_e; t_m)$ to denote the numbers of elementary MC steps for discarding and measurement. For the lattice size shown in Fig. 1, the times used were $(t_e = N;\ t_m = 2N)$, which correspond to 85 184 and 170 368 elementary MC steps (PT attempts plus Metropolis lattice sweeps), respectively. From this figure, it is apparent that good equilibration for the measurement process is achieved, even if half the above time is used.

Similarly, Fig. 2 presents the relaxation of cumulative moving averages for the sample averaging process of magnetization ($M = [\langle|M|\rangle]_s$ with $s = 1, \ldots, 200$), corresponding to the same lattice and the same temperature used for Fig. 1 and a total of 200 realizations. The sample-to-sample fluctuations (indicated by the dashed lines in Fig. 2) are, in general, larger than the statistical errors of the previous thermal averaging process (dotted lines in Fig. 1). The PT protocol is repeated several times by using new sets of temperatures and new realizations, and a final sufficiently dense set of points is obtained. The accuracy of the final MC data and the locations of the finite-size anomalies used in our FSS attempts depend on the detailed simulation conditions. The quality of the data should be reflected in the shapes of the finite-size peaks of the relevant thermodynamic quantities and can be observed from the characteristic examples that are presented in Sec. III B.

For each lattice size, we used several independent runs of large numbers of disorder realizations in order to obtain, in the temperature range of interest, the averaged curves $[Z]$, where Z denotes the thermal average of some thermodynamic quantity. In these runs, we use, in general, different temperature sequences consisting of three temperatures, corresponding to a PT exchange rate of 0.5. For the lattice sizes $L = 8, 12$, we used ten runs, each one consisting of 1000 realizations, and for the thermal process, we used the times $(t_e = 7N;\ t_m = 20N)$. For sizes $L = 16, 20, 24$, we used eight runs, each one consisting of 1000 realizations with times $(t_e = 5N;\ t_m = 15N)$. For the size $L = 28$, we used eight runs of 500 realizations with times $(t_e = 3N;\ t_m = 8N)$. For sizes $L = 32, 36, 40$, we used five runs, each one consisting of 300 realizations with times $(t_e = 2N;\ t_m = 5N)$. Finally, for $L = 44$, we used eight runs, each one consisting of 200 realizations with times $(t_e = N;\ t_m = 2N)$.

B. Finite-size scaling scheme

In the standard approach of FSS for a random system, a large number of disorder realizations has to be used in the summations in order to obtain good sample averages of the basic thermodynamic quantities Z, which are the usual thermal averages of a single disorder realization. From the disorder averages $[Z]$, we obtain their finite-size anomalies, denoted here as $[Z]^*$. These finite-size anomalies will be used in our FSS attempts following a quite common practice [63]. Their temperature locations, denoted by $T_{[Z]^*}$, will be used in the following in our FSS attempts. Thus, our paper concerns the critical exponents, describing the disorder-averaged behavior, and we do not attempt a FSS analysis based on sample dependent pseudocritical temperatures. The latter is a more demanding alternative approach [64–66], which considers the individual sample dependent maxima (anomalies) and the corresponding sample dependent pseudocritical temperatures. Note that, for disordered systems, one could make, in principle, a clear distinction between typical and averaged exponents [65,66].

From the MC data, several pseudocritical temperatures may be estimated, corresponding to finite-size anomalies, and these are expected to follow a power-law shift behavior $T_{[Z]^*} = T_c + b_Z L^{-1/\nu}$. The traditionally used specific heat and magnetic susceptibility peaks as well as the peaks corresponding to the following logarithmic derivatives of the powers $n = 1, 2, 4$ of the order parameter with respect to the inverse temperature $K = 1/T$ [67]:

$$\frac{\partial \ln\langle M^n\rangle}{\partial K} = \frac{\langle M^n H\rangle}{\langle M^n\rangle} - \langle H\rangle, \tag{5}$$

and the peak corresponding to the absolute order-parameter derivative,

$$\frac{\partial\langle|M|\rangle}{\partial K} = \langle|M|H\rangle - \langle|M|\rangle\langle H\rangle \tag{6}$$

will be located and will be used in our fitting attempts.

The behavior of the maxima of the logarithmic derivatives of the powers $n = 1, 2, 4$ of the order parameter with respect to the inverse temperature, which, as is well known, scales as $\sim L^{1/\nu}$ with the system size [67], is seen to provide a smooth root for the estimation of the correlation length exponent ν. Once the exponent ν is well estimated, the behavior of the values of the peaks corresponding to the absolute order-parameter derivative, which scale as $\sim L^{(1-\beta)/\nu}$ with the system size [67], gives one route for the estimation of the magnetic exponent ratio β/ν.

The above described FSS scheme will be applied in Sec. III B for the anisotropic case of $p_z = 0$; $p_{xy} = 0.176$ using lattice sizes in the range of $L \in \{8\text{–}44\}$. For the estimation of the critical temperature, we will mainly use a simultaneous fitting approach of the several pseudocritical

temperatures mentioned above. Furthermore, from the MC data for the disorder-averaged magnetization, it is possible to also follow an optimum collapse method, which provides simultaneous estimates for the critical exponents β/ν, $1/\nu$, as well as the critical temperature T_c. Such an optimum collapse method, using the downhill simplex algorithm, has recently been published [68]. This application will be carried out in Sec. III B using the scaling hypothesis,

$$[\langle|M|\rangle] = M(T,L) = L^{-\beta/\nu} f[(T - T_c)L^{1/\nu}], \qquad (7)$$

and the disorder-averaged magnetization data. The above mentioned collapse method will also be used for the location of two phase diagram points in the next subsection.

III. RESULTS

A. Phase diagram

As mentioned in the Introduction, the global phase diagram of the isotropic spin-glass model, defined by Eqs. (1) and (2), separates the three distinctive phases, ferromagnetic, paramagnetic, and glassy phases. This phase diagram is reproduced here by the solid lines in Fig. 3 and the full symbols used (squares, asterisk, and dot). The full squares and the asterisk on the FP transition line (IM) are reproduced from the Hasenbusch *et al.* [9] paper. The transition lines meet in a multicritical point (M), denoted by the full dot, [18–23] and located along the Nishimori line [24–27] with coordinates $T_M = 1.6692(3)$ and $p_M = 0.231\,80(4)$ [18–21]. The full square, point B, corresponds to the isotropic model at $p = \frac{1}{2}$ [11,13–15,41–53] and is placed at the temperature $T_c = 1.109(10)$ [10]. The full square point A, separating, at $T = 0$, the ferromagnetic and spin-glass states, corresponds to the ground state calculations by Hartmann [54] [$p_A = 0.222(5)$]. The location of this point indicates a reentrant FG transition line. This was nicely verified by the finite-temperature paper

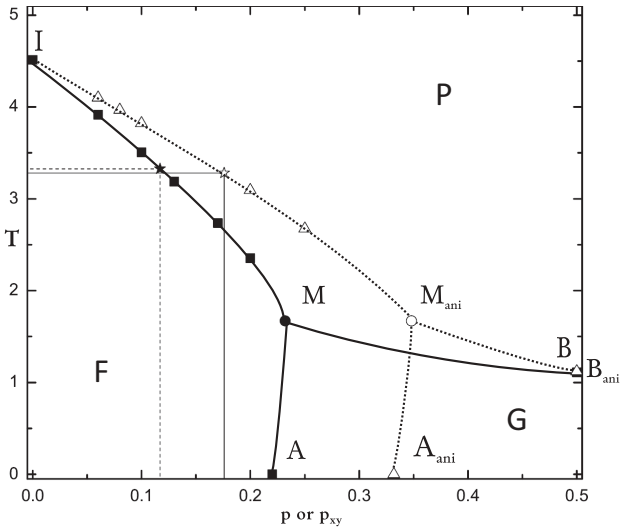

FIG. 3. Solid lines and full symbols: phase diagrams for the isotropic Edwards-Anderson model and dashed lines and open symbols: the present anisotropic model $p_z = 0, p_{xy}$. The phase diagram lines separate the three phases: F: ferromagnetic; G: spin-glass; and P: paramagnetic, which meet at dotted symbols: a multicritical point.

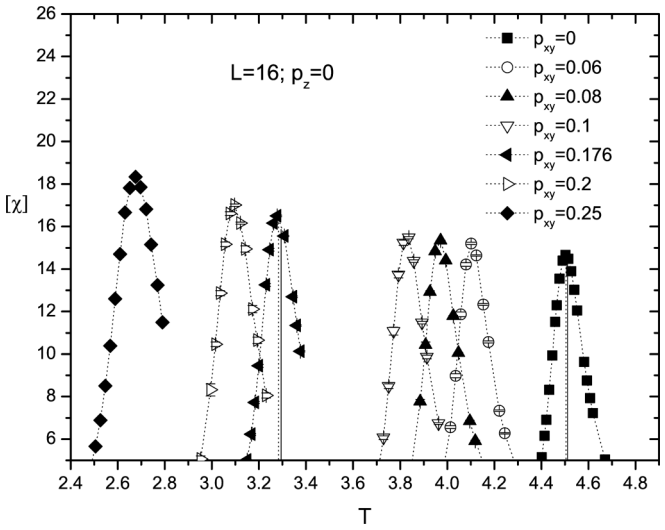

FIG. 4. Illustration of the magnetic susceptibility peaks for several cases of p_{xy} of the anisotropic model $p_z = 0$ for $L = 16$. Vertical drop lines demonstrate the differences between the dotted lines: $L = 16$ pseudocritical temperatures and the solid lines: corresponding asymptotic results for the pure Ising model $p_{xy} = 0$ and the anisotropic case $p_{xy} = 0.176$.

of Ceccarelli *et al.* [8] since they estimated $p(T = 0.5) = 0.2271(2)$ predicting the ferromagnetic-glassy transition line to be slightly reentrant. These results are in accordance with the Nishimori expectations [25,26] that this line cannot be forward and are also reflected in renormalization-group calculations [7,55,56].

Now, we give an approximate sketch of the global phase diagram of the anisotropic case (dashed lines and open symbols in Fig. 3). First, we consider its FP transition line ($IM_{\rm ani}$), and in Fig. 4, we present the numerical evidence for this line. The open triangle FP transition points, shown in Fig. 3, correspond to the cases of $p_z = 0$; $p_{xy} = 0.6,0.8,0.1,0.2,0.25$ and are obtained from the location of the peaks of the magnetic susceptibility for lattice size $L = 16$, illustrated in Fig. 4. In this figure, vertical drop lines have been used to demonstrate the difference between the present small-size ($L = 16$) pseudocritical temperatures and the corresponding asymptotic results for the pure Ising model ($p_{xy} = 0.0$) and the anisotropic case of $p_z = 0$; $p_{xy} = 0.176$. The asymptotic result for the pure Ising mode is $T_c = 4.511\,5232(16)$ [28–33] and is denoted by the full square on the phase diagram. The asymptotic result for the case of $p_z = 0$; $p_{xy} = 0.176$ is $T_c = 3.2938(9)$ (next subsection) and is denoted by the open asterisk on the phase diagram. Despite the small-size susceptibility approach followed here, the illustrated differences are small. The approximate sketch of the FP line is a reasonable approximation as results of the small temperature shifts in the magnetic susceptibilities of the systems.

Close to the Ising point, denoted by I in Fig. 3, the two FP lines (isotropic and anisotropic) appear to obey a smooth linear behavior. This linearity [$T_c(p) = T_c(0) - bp$] has been discussed and has been explained for the isotropic case by Hasenbusch *et al.* [9], and the corresponding slope (b_i) has been estimated. Their asymptotic estimates for the points $p = 0.0,0.6,0.1$, lead to an estimate on the order of $b_i \approx 2.2T_c \approx$

9.9 [9]. Following the present $L = 16$ susceptibility approach, we have estimated, for the same points, $b_i \approx 10.1$ only 2% shifted from the above asymptotic value. This serves as an additional test of the present small-size approximation of the FP line. The estimate of the slope for the anisotropic case (b_a), using the cases $p_{xy} = 0.0,0.6,0.1$, is $b_a \approx 6.7$. Thus, within the $L = 16$ approximation, the ratio of the slopes is approximately $b_i/b_a \approx 1.5$. This comparison illustrates that the FP transition of the anisotropic system takes place at the same temperature with the isotropic model when $p_{xy} \approx 1.5p$. In the phase diagrams of Fig. 3, the open asterisk on the FP line of the anisotropic model denotes the case of $p_z = 0$; $p_{xy} = 0.176$, and the full asterisk denotes the case of $p^* = 0.117$ of the isotropic model studied by Hasenbusch *et al.* [9]. The horizontal drop lines from the phase diagrams indicate that these two asterisks are about at the same temperature. The vertical drop lines point to their respective probabilities, which approximately satisfy the relation $p_{xy} = 1.5p$. Since $p_z = 0$, under these conditions, the two systems roughly have the same ratio of ferromagnetic to antiferromagnetic interactions. This observation also indicates a physically plausible explanation for the approximate relation between the FP lines presented in Fig. 3. As shown by Hasenbusch *et al.* [9], the full asterisk $p^* = 0.117(3)$ case is an improved model in which the leading scaling corrections vanish.

The open triangle point $A_{\rm ani}$, illustrated in the corresponding phase diagram, was obtained by ground state calculations on lattices with $L = 6,8,10$ where the data collapse method [68] was applied. Using a suitable PT protocol, we calculated the ground state ferromagnetic order parameter $M = [\langle |M| \rangle]$ for various values of p_{xy}. We used samples consisting of 10 000 realizations for each case and lattice size. The collapse of the data with the scaling hypothesis $M = L^{-\beta/\nu} f[(p_{xy} - p_c)L^{1/\nu}]$ is illustrated in Fig. 5, and the critical parameters are shown in the panel. According to this approximation, $A_{\rm ani}$ is located at $p_{A_{\rm ani}} = 0.332(12)$, very close to $p_{xy} = 1.5p$, where $p = p_A = 0.222(5)$ [54] is the point separating, in the isotropic case, the ferromagnetic and spin-glass states at $T = 0$. Hence, it appears that, again, as for the FP lines, the FG transitions of the isotropic and anisotropic systems

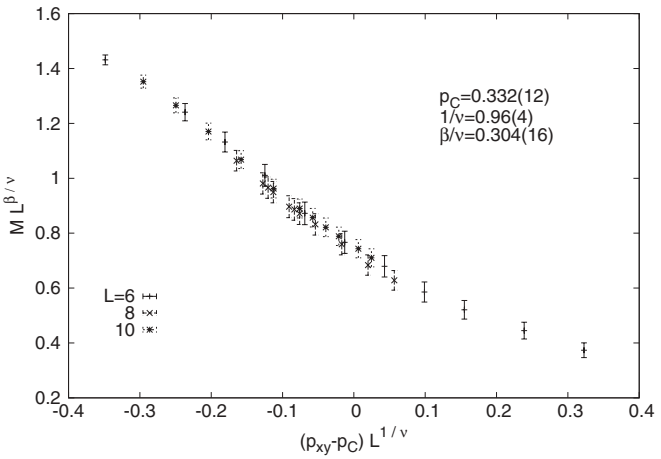

FIG. 5. Estimation via the collapse method of the phase diagram point $A_{\rm ani}$, separating, for the anisotropic model ($p_z = 0$), the ferromagnetic and spin-glass states at $T = 0$.

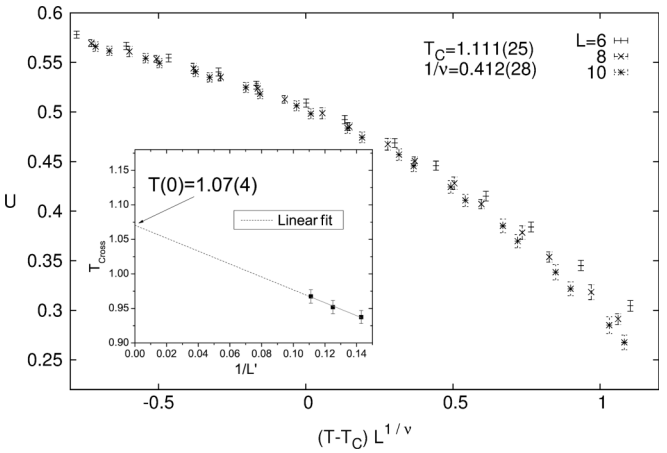

FIG. 6. Illustration of two methods for the estimation of the phase diagram point $B_{\rm ani}$. The inset illustrates a linear extrapolation of Binder's fourth-order cumulant crossing points of the spin-glass overlap order parameter. The main panel illustrates the collapse attempts for these Binder fourth-order cumulants.

approximately take place at $T = 0$ when the two systems approximately have the same ratio of ferromagnetic to antiferromagnetic interactions. It appears that the relation $p_{xy} = 1.5p$ gives a reasonable approximation for the FP as well as the FG transition lines and their crossing point. Thus, the multicritical point for the anisotropic case, shown as an open circle in Fig. 3, has been placed in the phase diagram by merely assuming that the two multicritical points are approximately at the same temperature and ratio of ferromagnetic to antiferromagnetic interactions. Using the known estimates for the isotropic multicritical point and the relation $p_{xy} = 1.5p$, we assert that $T_{M_{\rm ani}} = 1.669, \ldots$, $p_{M_{\rm ani}} = 0.3477, \ldots$. One should, of course, realize that this approximation is not expected to be accurate for the digits shown, and a separate detailed study is required for a better estimation.

We finally turn to the phase diagram point $B_{\rm ani}$ (open triangle), corresponding to the case of $p_z = 0$, $p_{xy} = \frac{1}{2}$, which appears to coincide with the isotopic phase diagram point B. In Fig. 6, we present the numerical evidence from our Monte Carlo data to locate this point. For a convenient range of temperatures, we generated data for the Binder's fourth-order cumulant $[U = 1 - \frac{1}{3}(\frac{[\langle q^4 \rangle]}{[\langle q^2 \rangle]^2})]$ where $\langle \cdots \rangle$ and $[\cdots]$ denote thermal and disorder averages, respectively, and q denotes the spin-glass overlap order parameter ($q = \frac{1}{N}\sum_{i=1}^{N} s_i^\alpha s_i^\beta$, where s_i denotes the spin of site i and α and β represent two replicas of the same disorder realization). The data are collected by a PT protocol using samples consisting of 10 000 realizations for lattice sizes $L = 6$, 8, and 2000 for $L = 10$. Using these data, the estimation of $B_{\rm ani}$ can be attempted by two methods. The inset of Fig. 6 illustrates a linear extrapolation of the crossing points of Binder's fourth-order cumulants. The fit is performed in $1/L'$ with $L' = \{\frac{(L_6+L_8)}{2}, \frac{(L_6+L_{10})}{2}, \frac{(L_8+L_{10})}{2}\}$ and gives the estimate $T_{B_{\rm ani}} = 1.07(4)$. Furthermore, in the main panel of Fig. 6, we illustrate the quality of the data collapse for Binder's fourth-order cumulants, and we give the estimated optimal critical parameters. The critical temperature estimate $T_{B_{\rm ani}} = 1.111(25)$ is very close to the corresponding estimate of the isotropic case $T_B = 1.109(10)$ [10]. Our finding appears to

be an interesting and physically appealing prediction, a proof that $T_B = T_{B_{\rm ani}}$ may help in better understanding the general universality question. In closing this discussion, we point out that the introduction of anisotropy changes the phase diagram and may also change the symmetry of the multicritical points as discussed by Güven *et al.* [7]. In general, the multicritical points, such as in the present model case ($p_z = 0$; $p_{xy} \leqslant \frac{1}{2}$), do not necessarily obey Nishimori conditions, and one cannot exclude the possibility of a ferromagnetic-glassy transition line being forward.

B. Estimation of critical behavior

In this subsection, we present a detailed FSS analysis for the case of $p_z = 0$; $p_{xy} = 0.176$ and provide sufficient evidence that the present anisotropic model belongs to the universality class of RIM. We will follow the FSS scheme described in Sec. II B using the MC data obtained for lattice sizes in the range of $L \in \{8\text{–}44\}$ according to the detailed simulation conditions summarized at the end of Sec. II A.

We start by analyzing the finite-size anomalies of the sample average of the logarithmic derivatives of the powers ($n = 1,2,4$) of the order parameter with respect to the inverse temperature. In Fig. 7, we illustrate the peaks of the $n = 4$ logarithmic derivatives for the larger lattice sizes $L \in \{20\text{–}44\}$. The shape of these peaks is smooth, reflecting the quality of the MC data. Assuming that these finite-size anomalies ($[Z]^*$) of the disorder averages $[Z]$, where Z is the thermal average given by Eq. (5), scale as $\sim L^{1/\nu}$ with the system size [67], in Figs. 8 and 9, we estimate this exponent. A very good scaling behavior is already observed by using the whole size range of our Monte Carlo data $L = [8\text{–}44]$. The simultaneous fitting attempt to the expected power-law behavior, illustrated in Fig. 8, gives the estimate shown in the panel: $1/\nu = 1.468(6)$.

By varying the $L_{\rm min}$ in these simultaneous fitting attempts, we obtain a sequence of effective exponents, depending on the minimum size used ($L_{\rm min} = [8\text{–}24]$). The behavior of these effective exponents is shown in Fig. 9. The smooth, almost linear, behavior of these effective exponents enables us to confinedly estimate $1/\nu = 1.463(3)$. The error range of this estimation is also indicated in Fig. 9 by the dotted lines and is compared with the corresponding three-dimensional (3D) pure Ising model for which an extremely accurate estimation is available [28]. The present estimate for the correlation length exponent $\nu = 0.6835(25)$ compares well with the estimate $\nu = 0.683(3)$ of Hasenbusch *et al.* [9] for the corresponding isotropic $\pm J$ Ising model at the ferromagnetic-paramagnetic transition line and is in excellent agreement with the estimate $\nu = 0.6837(53)$ of the extensive numerical investigations of Ballesteros *et al.* [35] for the site-diluted Ising model.

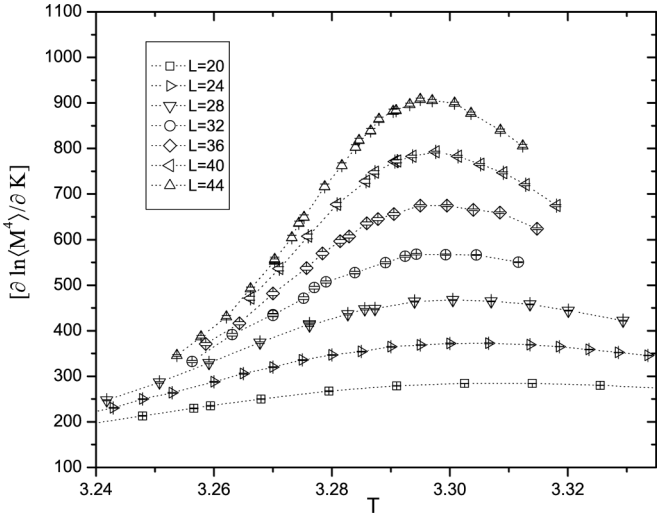

FIG. 7. Illustration of the peaks of the $n = 4$ logarithmic derivatives of the order parameter, using the MC data for sizes $L = 20\text{–}44$.

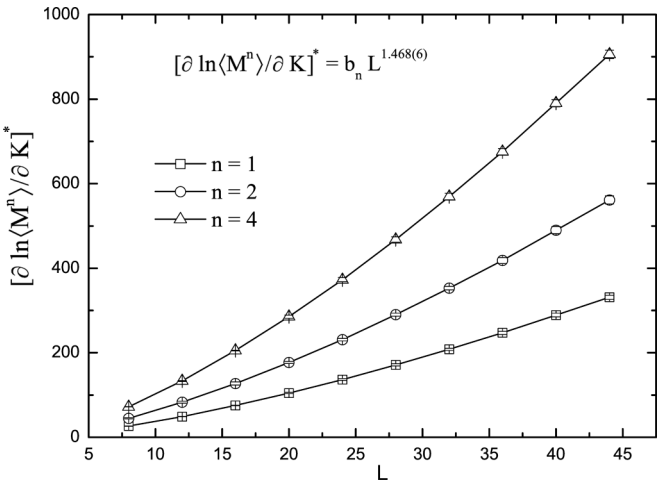

FIG. 8. FSS behavior of the peaks of the logarithmic derivatives of the powers $n = 1,2,4$ of the order parameter with respect to the inverse temperature. The estimate for the exponent $1/\nu = 1.468(6)$ (shown in the panel) is obtained by applying a simultaneous fitting attempt to a simple power law in the whole size range of $L = 8\text{–}44$.

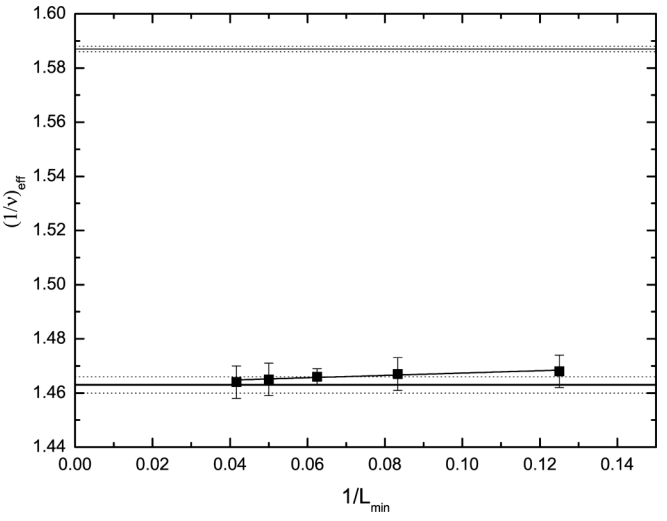

FIG. 9. Illustration of the behavior of the effective exponents $(1/\nu)_{\rm eff}$. The solid line drawn in the panel together with the dotted lines indicate the critical exponent range for the present model. The linear behavior illustrated gives the accurate estimation $1/\nu = 1.463(3)$. For comparison, the analogous narrow range of $1/\nu = 1.587(1)$ [28] for the pure 3D Ising model is shown in the upper part of the panel.

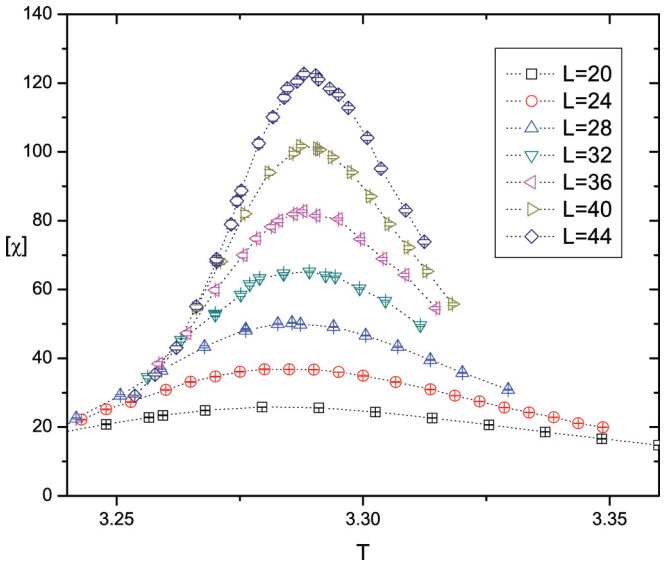

FIG. 10. (Color online) Illustration of the sample-averaged susceptibility peaks, using the MC data for sizes $L = 20$–44.

Next, we proceed to calculate the critical exponent ratio γ/ν from the peaks of the sample-averaged susceptibility ($[\chi]^*$). Again, in Fig. 10, we illustrate the quality of our MC data by presenting the peaks of the sample-averaged susceptibility. We assume that these finite-size anomalies obey a simple power law: $[\chi]^* = bL^{\gamma/\nu}$ and, again, follow the practice of observing the behavior of effective exponents by varying the $L_{\min}$ of the fitting range. In Fig. 11, we illustrate the effective exponent, obtained by applying the above power law for $L_{\min} = 8$. The resulting sequence of effective exponents ($L_{\min} = [8–24]$) is illustrated in Fig. 12. As seen from this figure, the illustrated linear fit gives the estimate $\gamma/\nu = 1.9614(28)$, which is consistent with that of Ballesteros *et al.* [35], $\gamma/\nu = 1.963(5)$, and those of Hasenbusch *et al.* [36], 1.964(1), for the

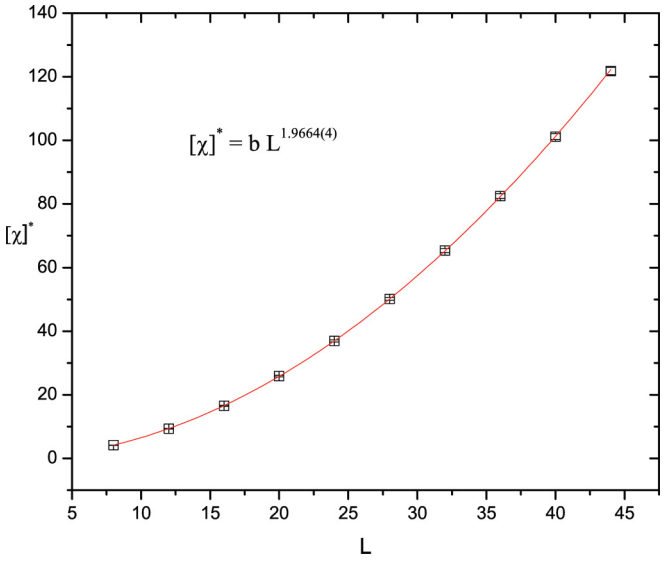

FIG. 11. (Color online) FSS behavior of the peaks of the magnetic susceptibility. The estimate for the exponent $\gamma/\nu = 1.966(4)$ (shown in the panel) is obtained by fitting a simple power law in the entire size range of $L = 8$–44.

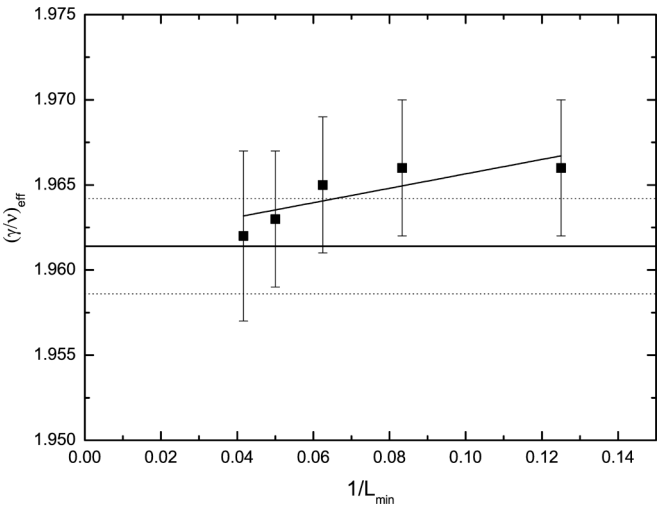

FIG. 12. For the behavior of the effective exponents γ/ν, the solid line, drawn through the points, is a linear fit. Solid and dotted lines indicate the corresponding critical exponent range $\gamma/\nu = 1.9614(28)$.

site-diluted 3D Ising model and 1.964(2) [9] for the isotropic $\pm J$ Ising model at the ferromagnetic-paramagnetic transition line. The observed variation in the estimates in Fig. 12 shows that, for the anisotropic case, leading scaling corrections may not vanish.

We now attempt the estimation of the exponent ratio β/ν via the scaling behavior of the peaks, corresponding to the absolute order-parameter derivative, which is expected to scale as $[\partial\langle|M|\rangle/\partial K]^* = bL^{(1-\beta)/\nu}$. As before, in Fig. 13, we illustrate the smooth behavior of the peaks of the absolute order-parameter derivative. Figure 14 shows the effective exponent obtained by fitting the above mentioned power law to the entire size range of $L = [8–44]$. The corresponding effective exponent estimates are illustrated in Fig. 15. The linear fit, illustrated in this figure, gives $(1 - \beta)/\nu = 0.9572(54)$, which, by using our estimate $1/\nu = 1.463(3)$, produces, for β/ν, the

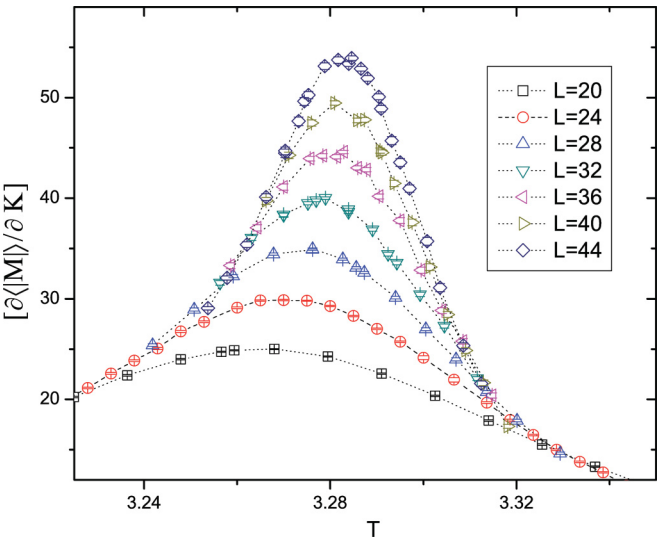

FIG. 13. (Color online) Illustration of the peaks of the absolute order-parameter derivative, using the MC data for $L = 20$–44.

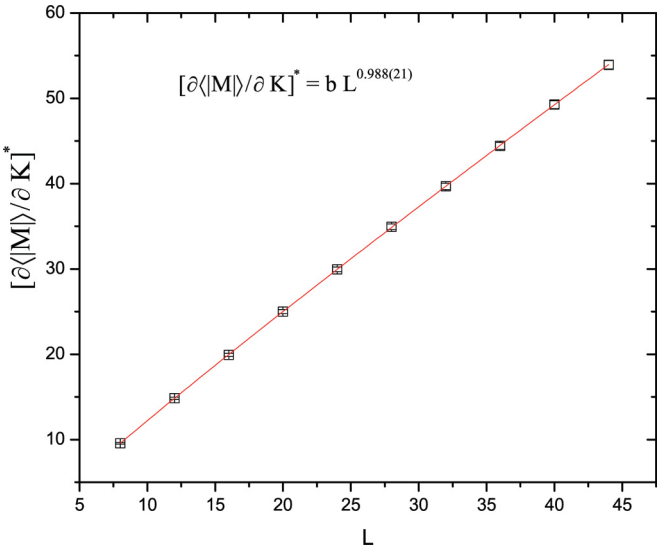

FIG. 14. (Color online) FSS behavior of the peaks of the derivatives of the absolute order parameter with respect to the inverse temperature. The estimate for the exponent $(1-\beta)/\nu = 0.988(21)$ (shown in the panel) is obtained by fitting a simple power law in the whole size range of $L = 8$–44.

range 0.5058(84). This value is somewhat smaller than the value $\beta/\nu = 0.518$, expected from hyperscaling and accepting an estimate for γ/ν on the order of the above mentioned literature estimates (say, for instance, $\gamma/\nu = 1.964$). The situation is improved by attempting the linear fit in Fig. 15 only at the last three points. The linear fit in these three points ($L_{\min} = 16,20,24$) gives $(1-\beta)/\nu = 0.948(3)$ producing, as above, $\beta/\nu = 0.515(6)$. Note also that the second-order polynomial fit, also shown in Fig. 15 and applied to all five points, gives an estimate $(1-\beta)/\nu = 0.943(6)$ now producing

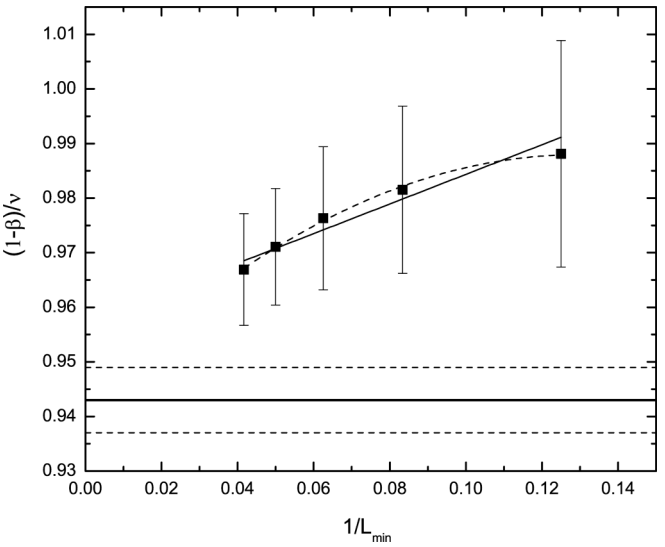

FIG. 15. Illustration of the behavior of the effective exponents $(1-\beta)/\nu$. The solid and the dashed lines, drawn through the points, indicate linear and second-order polynomial fits. The critical exponent range for the latter fit is indicated by the solid and dotted lines at $(1-\beta)/\nu = 0.943(6)$.

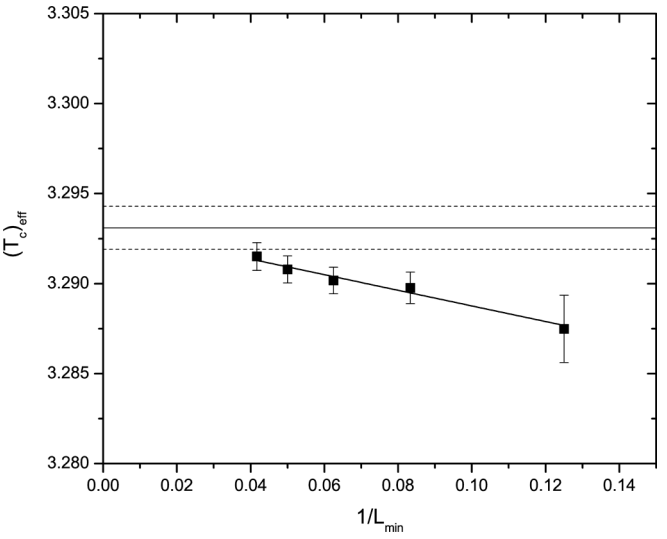

FIG. 16. Behavior of the effective pseudocritical temperatures obtained by applying a simultaneous fit on the shift behavior $T_{[Z]^*} = T_c + b_Z L^{-1/\nu}$ and fixing the exponents to the accurate estimate $1/\nu = 1.463$. The solid and dotted lines indicate the critical temperature range $T_c = 3.2931(12)$, obtained by the illustrated linear fit.

$\beta/\nu = 0.520(9)$. These last values are in good accordance with hyperscaling and the literature estimate of γ/ν.

The critical temperature will now be estimated by a simultaneous fitting approach, using several pseudocritical temperatures of the sample average of the quantities measured [58,69] as outlined earlier. The simultaneous fitting is attempted for the expected power-law shift behavior $T_{[Z]^*} = T_c + b_Z L^{-1/\nu}$ for the six pseudocritical temperatures mentioned in the previous section.

We approach this estimation by simultaneous fittings in which we are fixing the exponent $1/\nu$ to the apparently accurate estimate $1/\nu = 1.463$. Following our earlier practice of using different fitting ranges by varying the $L_{\min}$ of the fitting range, we obtain a sequence of estimates illustrated in Fig. 16. The linear fit shown in the panel gives an estimate of $T_c = 3.2931(12)$, illustrated with solid and dotted lines in this figure, whereas, restricting the fit only to the last three points, corresponding to $L_{\min} = 16,20,24$, gives a higher estimate $T_c = 3.2945(18)$. We note here that a completely free fit, without fixing any parameter and following the above practice, gives $T_c = 3.2934(8)$ from the linear fit to the five points $L_{\min} = 8,12,16,20,24$ and $T_c = 3.2940(16)$ from the linear fit to the three points $L_{\min} = 16,20,24$. Thus, we suggest that $T_c = 3.2938(9)$, which satisfies all the previous estimates.

Finally, we present the alternative estimation of critical behavior by studying the expected scaling law Eq. (7) for the order-parameter data, here, the disorder-averaged magnetization data. Using the earlier mentioned collapse method, we rescale the y axis to $ML^{\beta/\nu}$ and the x to $(T-T_c)L^{1/\nu}$, and we attempt to observe the optimum collapse of the magnetization curves taken from different lattice sizes ($L = [12$–$44]$). We apply the downhill simplex algorithm as developed and implemented in Ref. [68] for the estimation of critical properties and their error bounds. As shown in the panel of Fig. 17, the optimum collapse gives $\beta/\nu = 0.516(7)$. This value is in good agreement with the expected value. The

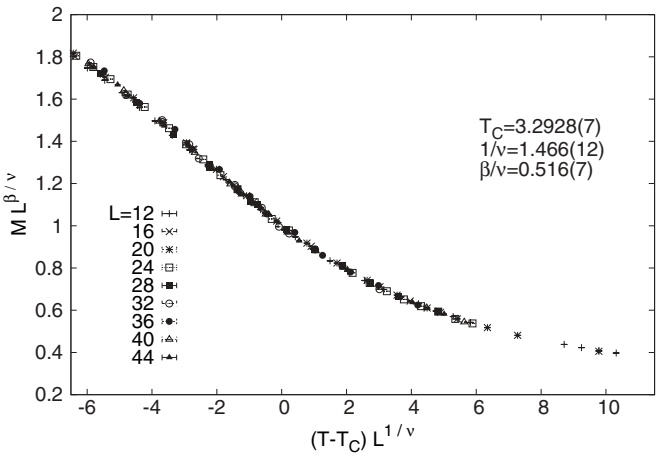

FIG. 17. Illustration of magnetization data collapse for lattice sizes of $L = 12$–44. The collapse method is applied to the whole range shown and gives the values $T_c = 3.2928(7)$, $1/\nu = 1.466(12)$, and $\beta/\nu = 0.516(7)$.

resulting estimates for the exponent $1/\nu = 1.466(12)$ and the estimate for the critical temperature $T_c = 3.2928(7)$ are in fair agreement with our previous findings. However, the estimate $\beta/\nu = 0.516(7)$ appears to be very satisfactory.

IV. CONCLUSIONS

The present paper clearly pointed out that the $\pm J$ three-dimensional Ising model, with spatially uniaxial anisotropic bond randomness, gives rise to a second-order phase transition belonging in the same universality class as the 3D random Ising model. The implemented anisotropy appears as an irrelevant parameter for the ferromagnetic-paramagnetic transition line. We found the reliable estimates $\beta/\nu = 0.516(7)$ by using the collapse method of Ref. [68] and $\nu = 0.6835(25)$ from the smooth behavior of the logarithmic derivatives of the order parameter. We have also presented a conjectured global phase diagram, providing interesting predictions.

Currently, we are carrying out further numerical simulations. From these, it seems that, here, the implemented anisotropy ($p_z = 0$; $J^z = J^{xy}$) is also an irrelevant parameter for the two other transition lines of the phase diagram. The reader can observe signs of this universality for the case of the ferromagnetic spin-glass transition by comparing the critical exponents in the panel of Fig. 5 with those of Ceccarelli *et al.* [8]. Furthermore, the critical exponent $1/\nu$ in the panel of Fig. 6 seems to agree with the estimates given by Katzgraber *et al.* [11] for the spin-glass paramagnetic transition. Finally, we are considering the more general case ($J^z \neq J^{xy}$). We hope that we will soon provide further confirmation of the discussed predictions in this paper and will observe and will verify the interesting features of the global phase diagrams brought out by the paper of Güven *et al.* [7].

ACKNOWLEDGMENTS

The authors are grateful to A. N. Berker for our constructive discussions on the subject. This work was supported by the special Account for Research of the University of Athens (Code No. 11112). T.P. has been supported by the Special Account of the University of Athens through a Ph.D. grant.

[1] A. Ito, H. Aruga, E. Torikai, M. Kikuchi, Y. Syono, and H. Takei, Phys. Rev. Lett. **57**, 483 (1986).
[2] K. Gunnarsson, P. Svedlindh, P. Nordblad, L. Lundgren, H. Aruga, and A. Ito, Phys. Rev. B **43**, 8199 (1991).
[3] S. Nair and A. K. Nigam, Phys. Rev. B **75**, 214415 (2007).
[4] J. J. Hopfield, Proc. Natl. Acad. Sci. USA **79**, 2554 (1982).
[5] S. F. Edwards and P. W. Anderson, J. Phys. F **5**, 965 (1975).
[6] K. Binder and A. P. Young, Rev. Mod. Phys. **58**, 801 (1986).
[7] C. Güven, A. N. Berker, M. Hinczewski, and H. Nishimori, Phys. Rev. E **77**, 061110 (2008).
[8] G. Ceccarelli, A. Pelissetto, and E. Vicari, Phys. Rev. B **84**, 134202 (2011).
[9] M. Hasenbusch, F. Parisen Toldin, A. Pelissetto, and E. Vicari, Phys. Rev. B **76**, 094402 (2007).
[10] M. Hasenbusch, A. Pelissetto, and E. Vicari, Phys. Rev. B **78**, 214205 (2008).
[11] H. G. Katzgraber, M. Körner, and A. P. Young, Phys. Rev. B **73**, 224432 (2006).
[12] T. Jörg, Phys. Rev. B **73**, 224431 (2006).
[13] I. A. Campbell, K. Hukushima, and H. Takayama, Phys. Rev. B **76**, 134421 (2007).
[14] H. G. Ballesteros, A. Cruz, L. A. Fernández, V. Martín-Mayor, J. Pech, J. J. Ruiz-Lorenzo, A. Tarancón, P. Téllez, C. L. Ullod, and C. Ungil, Phys. Rev. B **62**, 14237 (2000).
[15] M. Palassini and S. Caracciolo, Phys. Rev. Lett. **82**, 5128 (1999).
[16] N. Kawashima and H. Rieger, in *Frustrated Spin Systems*, edited by H. T. Diep (World Scientific, Singapore, 2005).
[17] A. Billoire, L. A. Fernandez, A. Maiorano, E. Marinari, V. Martín-Mayor, and D. Yllanes, J. Stat. Mech.: Theory Exp. (2011) P10019.
[18] M. Hasenbusch, F. Parisen Toldin, A. Pelissetto, and E. Vicari, Phys. Rev. B **76**, 184202 (2007).
[19] Y. Ozeki and H. Nishimori, J. Phy. Soc. Jpn. **56**, 3265 (1987).
[20] Y. Ozeki and N. Ito, J. Phys. A **31**, 5451 (1998).
[21] R. R. P. Singh, Phys. Rev. Lett. **67**, 899 (1991).
[22] P. Le Doussal and A. B. Harris, Phys. Rev. Lett. **61**, 625 (1988).
[23] P. Le Doussal and A. B. Harris, Phys. Rev. B **40**, 9249 (1989).
[24] H. Nishimori, *Statistical Physics of Spin Glasses and Information Processing: An Introduction*, International Series of Monographs on Physics (Oxford University Press, New York, 2001).
[25] H. Nishimori, J. Phys. C **13**, 4071 (1980).
[26] H. Nishimori, Prog. Theor. Phys. **66**, 1169 (1981).
[27] H. Nishimori, J. Phys. Soc. Jpn. **55**, 3305 (1986).
[28] M. Hasenbusch, Phys. Rev. B **82**, 174433 (2010).
[29] M. Campostrini, A. Pelissetto, P. Rossi, and E. Vicari, Phys. Rev. E **65**, 066127 (2002).
[30] R. Guida and J. Zinn-Justin, J. Phys. A **31**, 8103 (1998).

[31] P. Butera and M. Comi, Phys. Rev. B **65**, 144431 (2002).
[32] Y. Deng and H. W. J. Blöte, Phys. Rev. E **68**, 036125 (2003).
[33] H. W. J. Blote, E. Luijten, and J. R. Heringa, J. Phys. A **28**, 6289 (1995).
[34] K. Hukushima, J. Phys. Soc. Jpn. **69**, 631 (2000).
[35] H. G. Ballesteros, L. A. Fernández, V. Martín-Mayor, A. Muñoz Sudupe, G. Parisi, and J. J. Ruiz-Lorenzo, Phys. Rev. B **58**, 2740 (1998).
[36] M. Hasenbusch, F. Parisen Toldin, A. Pelissetto, and E. Vicari, J. Stat. Mech.: Theory Exp. (2007) P02016.
[37] A. Pelissetto and E. Vicari, Phys. Rev. B **62**, 6393 (2000).
[38] P. E. Berche, C. Chatelain, B. Berche, and W. Janke, Eur. Phys. J. B **38**, 463 (2004).
[39] P. E. Theodorakis and N. G. Fytas, Eur. Phys. J. B **81**, 245 (2011).
[40] A. Malakis, A. N. Berker, N. G. Fytas, and T. Papakonstantinou, Phys. Rev. E **85**, 061106 (2012).
[41] A. T. Ogielski and I. Morgenstern, Phys. Rev. Lett. **54**, 928 (1985).
[42] A. T. Ogielski, Phys. Rev. B **32**, 7384 (1985).
[43] R. R. P. Singh and S. Chakravarty, Phys. Rev. Lett. **57**, 245 (1986).
[44] R. N. Bhatt and A. P. Young, Phys. Rev. Lett. **54**, 924 (1985).
[45] N. Kawashima and A. P. Young, Phys. Rev. B **53**, R484 (1996).
[46] L. W. Bernardi, S. Prakash, and I. A. Campbell, Phys. Rev. Lett. **77**, 2798 (1996).
[47] B. A. Berg and W. Jahnke, Phys. Rev. Lett. **80**, 4771 (1998).
[48] P. O. Mari and I. A. Campbell, Phys. Rev. E **59**, 2653 (1999).
[49] P. O. Mari and I. A. Campbell, arXiv:cond-mat/0111174.
[50] P. O. Mari and I. A. Campbell, Phys. Rev. B **65**, 184409 (2002).
[51] T. Nakamura, S.-i. Endoh, and T. Yamamoto, J. Phys. A **36**, 10895 (2003).
[52] M. Pleimling and I. A. Campbell, Phys. Rev. B **72**, 184429 (2005).
[53] I. A. Campbell, K. Hukushima, and H. Takayama, Phys. Rev. Lett. **97**, 117202 (2006).
[54] A. K. Hartmann, Phys. Rev. B **59**, 3617 (1999).
[55] G. Migliorini and A. N. Berker, Phys. Rev. B **57**, 426 (1998).
[56] M. Hinczewski and A. N. Berker, Phys. Rev. B **72**, 144402 (2005).
[57] N. Metropolis, A. W. Rosenbluth, M. N. Rosenbluth, A. H. Teller, and E. Teller, J. Chem. Phys. **21**, 1087 (1953).
[58] A. Malakis, G. Gulpinar, Y. Karaaslan, T. Papakonstantinou, and G. Aslan, Phys. Rev. E **85**, 031146 (2012).
[59] E. Bittner, A. Nußbaumer, and W. Janke, Phys. Rev. Lett. **101**, 130603 (2008).
[60] R. H. Swendsen and J. S. Wang, Phys. Rev. Lett. **58**, 86 (1987); U. Wolff, *ibid.* **62**, 361 (1989).
[61] M. E. J. Newman and G. T. Barkema, *Monte Carlo Methods in Statistical Physics* (Clarendon, Oxford, 1999).
[62] D. P. Landau and K. Binder, *Monte Carlo Simulations in Statistical Physics* (Cambridge University Press, Cambridge, UK, 2000).
[63] C. Chatelain, B. Berche, W. Janke, and P. E. Berche, Phys. Rev. E **64**, 036120 (2001); Nucl. Phys. B **719**, 725 (2005).
[64] S. Wiseman and E. Domany, Phys. Rev. Lett. **81**, 22 (1998); Phys. Rev. E **58**, 2938 (1998).
[65] D. S. Fisher, Phys. Rev. B **51**, 6411 (1995).
[66] J. T. Chayes, L. Chayes, D. S. Fisher, and T. Spencer, Phys. Rev. Lett. **57**, 2999 (1986); Commun. Math. Phys. **120**, 501 (1989).
[67] A. M. Ferrenberg and D. P. Landau, Phys. Rev. B **44**, 5081 (1991).
[68] O. Melchert, arXiv:0910.5403.
[69] A. Malakis, A. N. Berker, I. A. Hadjiagapiou, and N. G. Fytas, Phys. Rev. E **79**, 011125 (2009).